Journal of Colloid and Interface Science 433 (2014) 211–217

Contents lists available at ScienceDirect

Journal of Colloid and Interface Science

www.elsevier.com/locate/jcis

Simple sol–gel process to obtain silica-coated anatase particles with enhanced TiO_2-SiO_2 interfacial area

S.F. Resende *, E.H.M. Nunes, M. Houmard, W.L. Vasconcelos

Universidade Federal de Minas Gerais, Av. Antônio Carlos, 6627, Pampulha, Belo Horizonte, Brazil

ARTICLE INFO

Article history:
Received 20 March 2014
Accepted 16 June 2014
Available online 22 June 2014

Keywords:
Anatase particles
Silica coating
Sol-gel
Hydrothermal treatment
TiO_2-SiO_2 interfaces

ABSTRACT

In this study we prepared silica-titania composites with a low SiO_2:TiO_2 molar ratio. These materials were prepared using a simple sol–gel route in which a hydrothermal treatment was used to obtain mesoporous anatase particles. Pure titania was also synthetized for comparison purposes. These materials were examined by scanning and transmission electron microscopy (SEM and TEM, respectively), energy dispersive X-ray spectroscopy (EDS), X-ray diffraction (XRD), Fourier transform infrared spectroscopy (FTIR), differential scanning calorimetry (DSC), and nitrogen sorption tests. A thin silica coating was formed on the anatase particles. It was observed that the presence of this coating led to samples with an enhanced thermal stability. Indeed, the composites prepared in this work showed an anatase structure and a high specific surface area (SSA), even after their calcination at 800 °C. Thus, we believe that the synthetized material present an outstanding SiO_2-TiO_2 interfacial area associated with a high amount of anatase particles which could improve its photoactive properties.

1. Introduction

TiO_2 has been used in many applications, including solar energy conversion [1], H_2 and O_2 production [2], microorganism removal [3], odor control [4], photocatalysis [5], and self-cleaning surfaces [6]. The photoinduced properties of TiO_2 have been widely investigated over the last years. One of the most interesting aspects concerning these properties is related to the fact that the photocatalysis and photoinduced super-hydrophilicity of TiO_2 can act in synergy [7–9]. The photoinduced properties of TiO_2 are related to its physicochemical properties, including crystal structure, particle size, and specific surface area (SSA) [10]. It is well established that anatase usually shows a higher photoactivity than rutile. This behavior is partly associated with the faster electron–hole recombination process exhibited by anatase [11,12]. Moreover, anatase is usually obtained at temperatures below 600 °C, which leads to the formation of small particles with large SSA and high density of active sites [13].

The use of TiO_2 nanoparticles at high temperatures could decrease their SSA due to the occurrence of phase transformation and crystal growth [14,15]. In attempting to overcome this drawback many authors have incorporated oxide phases such as SiO_2, ZrO_2, and Al_2O_3 into the titania structure [16–18]. It is well known that the addition of SiO_2 to titania improves the surface area available for catalysis, allowing the adsorption of pollutants in many applications [19]. Furthermore, several works have reported that the presence of SiO_2 inhibits the TiO_2 crystallization [20–22]. Guan et al. [23] suggested that the addition of silica may increase the concentration of hydroxyl groups on the titania surface, leading to samples with enhanced hydrophilic and photocatalytic properties. This effect could be related to the formation of TiO_x^- and SiO_x^+ groups at TiO_2-SiO_2 interfaces. Perpoom et al. [24] and Houmard et al. [25,26] reported that these groups could lead to a natural, photo-regenerated, and persistent superhydrophilicity in the TiO_2-SiO_2 composite.

Several works found in the literature regarding TiO_2-SiO_2 composites deal with the fabrication of these materials by embedding anatase particles into a silica matrix [27,28]. However, this approach usually leads to samples with a low concentration of anatase particles and a small TiO_2-SiO_2 specific interfacial area. In this study we prepared silica-titania composites with a high TiO_2-SiO_2 interfacial area and a low SiO_2/TiO_2 ratio. These materials were prepared using a simple sol–gel route in which a hydrothermal treatment was used to obtain mesoporous anatase particles. Pure titania was also synthetized for comparison purposes. These materials were examined by scanning and transmission electron microscopy (SEM and TEM, respectively), energy dispersive X-ray spectroscopy (EDS), X-ray diffraction (XRD), Fourier transform infrared spectroscopy (FTIR), differential scanning calorimetry (DSC), and nitrogen sorption tests.

* Corresponding author.
E-mail address: susanaresendeufmg@gmail.com (S.F. Resende).

http://dx.doi.org/10.1016/j.jcis.2014.06.033
0021-9797/

2. Materials and methods

2.1. Synthesis

TiO_2 anatase nanoparticles were fabricated by methodology similar to that reported by Kim and Kwak [29]. Briefly, Pluronic P123 triblock copolymer ($EO_{20}PO_{70}EO_{20}$/Aldrich) was initially dissolved in deionized water at 40 °C. Next, sulfuric acid (H_2SO_4/99%/Aldrich) and a mixture of titanium tetraisopropoxide (TIPT/Aldrich) and 2,4-pentanedione (Aldrich) were added under strong stirring to the as-prepared solution. The solution was then kept at 55 °C for 2 h and, after several minutes, a light-yellow colored suspension was obtained. The hydrothermal treatment was carried out by aging the as-prepared suspension at 90 °C for 10 h. The obtained anatase nanoparticles were filtered and washed with water and absolute ethanol (EtOH/Aldrich/$\geqslant$99.5 %).

The SiO_2 sol was prepared according to the procedure described by Houmard et al. [25,26]. It was obtained by diluting tetraethylorthosilicate (TEOS/Aldrich/98%) in EtOH, deionized water, and hydrochloric acid (HCl/Aldrich/37%), with a TEOS concentration, H_2O:TEOS molar ratio (Rw), and pH of 2.35 M, 0.5, and 2, respectively. According to Houmard et al. [25,26,30], the synthesis conditions of this sol–gel solution could lead to a silica sol of low reactivity, favoring the reaction of silica particles on the titania surface. The TiO_2-SiO_2 composite was obtained by mixing the as-prepared silica sol with the previously fabricated anatase particles. The SiO_2:TiO_2 molar ratio was kept at 1:1. The suspension was sonicated for 30 min and then stirred overnight. Samples were eventually heat-treated in air at either 500 °C or 800 °C for 2 h. The heat treatment step was performed using a Lindberg/Blue furnace and a heating rate of 5 °C/min. As mentioned before, TiO_2 samples were also prepared for comparison purposes.

2.2. Characterization

Samples were examined in the as-prepared and heat-treated conditions. It is worth mentioning that samples in the as-prepared condition were hydrothermally treated at 90 °C and dried at 60 °C. For sake of clarity, as-prepared titania and silica-titania were denoted as TiO_2-As and TiO_2-SiO_2-As, respectively. Titania samples calcined at either 500 °C or 800 °C were designated as TiO_2-500 or TiO_2-800, respectively. Similarly, silica-titania specimens heated at 500 °C and 800 °C were denoted as TiO_2-SiO_2-500 and TiO_2-SiO_2-800.

SEM was performed with a FEI QUANTA 3D field emission gun scanning electron microscope (FEG-SEM). Samples were sputter-coated with a carbon layer of about 5 nm thickness before the SEM tests. EDS examinations were carried out using an OMEGAMAX EDS system available in an Aspex EXPLORER apparatus. Samples used in the EDS tests were deposited directly on carbon stubs and examined without further treatment. TEM was carried out using FEI TECNAI G2-12 SPIRITBIOTWIN and TECNAI G2-20 SUPERTWIN microscopes. Samples used in the TEM tests were previously dispersed in EtOH and sonicated for 5 min. Next, the obtained suspensions were dripped on carbon-coated TEM grids. After drying at room temperature, these grids were used in the TEM examinations.

XRD was carried out in a Philips-PANalytical PW17-10 diffractometer, using Cu Kα radiation and operating at 40 kV and 40 mA. XRD patterns were collected in the 2θ range of 10–90°, using a scan velocity of 0.06 °/min. The identification of the crystalline phases was performed using the JCPDS file numbers 21-1272 and 21-1276 for anatase and rutile, respectively. The TiO_2 crystallite size was assessed using the Scherrer equation and considering the XRD peaks at 25.3° and 27.5° for anatase and rutile, respectively.

DSC profiles were obtained with a Shimadzu DSC-50 thermal analysis system. These tests were performed using a heating rate of 10 °C/min and under air flow (20 mL/min). Nitrogen sorption tests were performed in a Micromeritics ASAP 2020 apparatus. Samples used in these analyses were previously degassed at 130 °C for up to 48 h under vacuum. The specific surface area (SSA) and pore size distribution were assessed by the multipoint BET and NLDFT methods, respectively. FTIR samples were prepared as pellets with KBr and examined in a Perkin-Elmer SPECTRUM 1000 spectrometer. The spectra were taken from 4000 cm^{-1} to 300 cm^{-1}, with a resolution of 4 cm^{-1} and 128 scans.

3. Results and discussion

3.1. XRD

Fig. 1 shows XRD patterns of samples obtained in this study. We noticed that anatase is the major phase present in the as-prepared samples. This finding reveals that the hydrothermal treatment allowed obtaining anatase particles at temperatures about 90 °C. According to Kim and Kwak [29], amorphous titania tends to become crystalline under high temperatures and pressures. The conversion of anatase to rutile was observed for pure titania when it was heat-treated at 800 °C. Nonetheless, this phase transformation was not observed for the silica–titania composite treated at the same temperature. This result suggests that the presence of silica inhibits the conversion of anatase to rutile, even when silica is present in low proportions (this point will be largely discussed in the next sections). This behavior could also indicate that it was formed a homogeneous silica layer on the titania particles, inhibiting the atom diffusion that leads to the anatase-to-rutile phase transition.

As mentioned before, the TiO_2 crystallite size was assessed using the Scherrer equation. TiO_2-As, TiO_2-500, and TiO_2-800 showed crystallite sizes of 11 nm, 19 nm, and 86 nm, respectively. On the other hand, TiO_2-SiO_2-As, TiO_2-SiO_2-500, and TiO_2-SiO_2-800 exhibited TiO_2 crystallites of 14 nm, 16 nm, and 43 nm, respectively. One notices that the crystallite size showed a slight increase upon heat treating samples at 500 °C. Nonetheless, it exhibited a significant increase when samples were calcined at 800 °C. This behavior was more pronounced for pure titania. This finding suggests that the silica coating increased the thermal stability of titania particles.

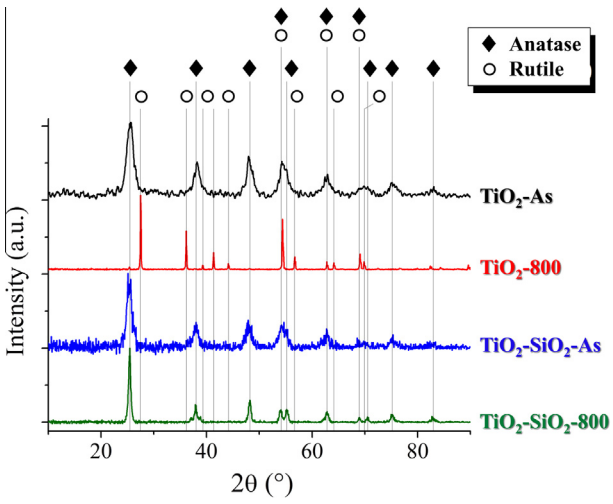

Fig. 1. XRD patterns of samples obtained in this study.

3.2. Imaging analyses

Fig. 2 shows SEM micrographs of titania and silica-titania samples in the as-prepared condition. We observed that the TiO_2 particles exhibited spherical shape with diameter of about 1 μm. This morphology could be associated with the use of P123 in the synthesis step. It is well established that P123 tends to form micelles when dispersed in aqueous solutions. Thus, the micelles formed in the sol–gel solution could lead to the orientation of Ti-O-Ti bonds, giving rise to spherical particles [31]. It was also noticed that the composite particles show morphology and size quite similar to those exhibited by the pure titania. Since the presence of silica on the titania surface apparently did not alter the particles size, one could suggest that the silica coating displays a small thickness.

Fig. 3 depicts EDS spectra of samples obtained in this work. TiO_2 exhibited peaks related to Ti and O, which reveals the formation of the titania framework. Intense peaks ascribed to C and S were also observed. We believe that they could be related to organic and sulfuric acid residues present in the samples structure from the synthesis step. The peak ascribed to C could also have a contribution from the carbon stubs in which samples were deposited before the EDS tests. One notices that the signal related to S was removed from samples upon calcination at 800 °C, whereas the signal related to C decreased in intensity after this heat treatment. The TiO_2-SiO_2 composite showed a signal associated with Si. This finding seems to reveal that a silica layer was successfully formed on the titania surface. It can also be observed that the Si peak is much less intense than those ascribed to Ti. This behavior shows that the silica-titania composite obtained in this work exhibits a low SiO_2:TiO_2 ratio. As aforementioned, this work was based on the procedure described by Houmard et al. [25,26] in attempting to obtain a poorly reactive SiO_2 sol. The low reactivity of the sol decreases the size of the silica oligomeric chains, favoring the

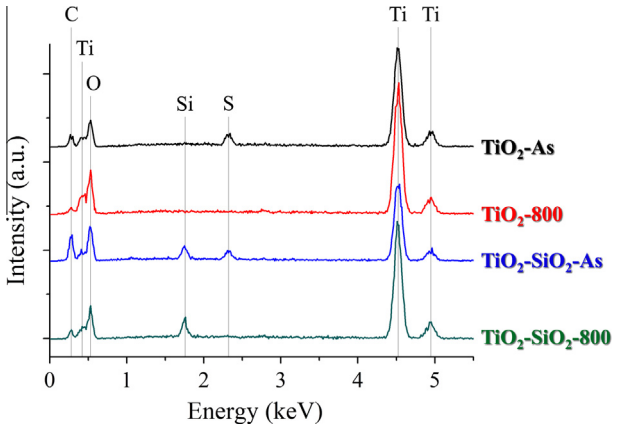

Fig. 3. EDS spectra of samples obtained in this study.

interaction of the SiO_2 on the TiO_2 particle surface. The reaction between adjacent silica chains is unlikely due to the low reactivity of the prepared SiO_2 sol. However, because of the lack of TiO_2 surface active sites available to graft all silica chains, the SiO_2 in excess was removed from samples during the filtration and washing steps. Thus, it is possible that the SiO_2-TiO_2 specific interfacial area has been maximized, i.e. all available titania sites have reacted with silica chains, which could improve the photoactive performance of the composite prepared in this study [32,33].

Figs. 4 and 5 exhibit TEM micrographs of TiO_2-As, TiO_2-800, TiO_2-SiO_2-As, and TiO_2-SiO_2-800. We observed that the particle size tended to increase when samples were heat-treated at 800 °C. Nonetheless, this behavior was more pronounced for pure titania, suggesting once again that the presence of the silica coating could inhibit the growth of the titania particles. It is possible to observe in Fig. 4III the crystal planes of rutile. From Fig. 5III, we

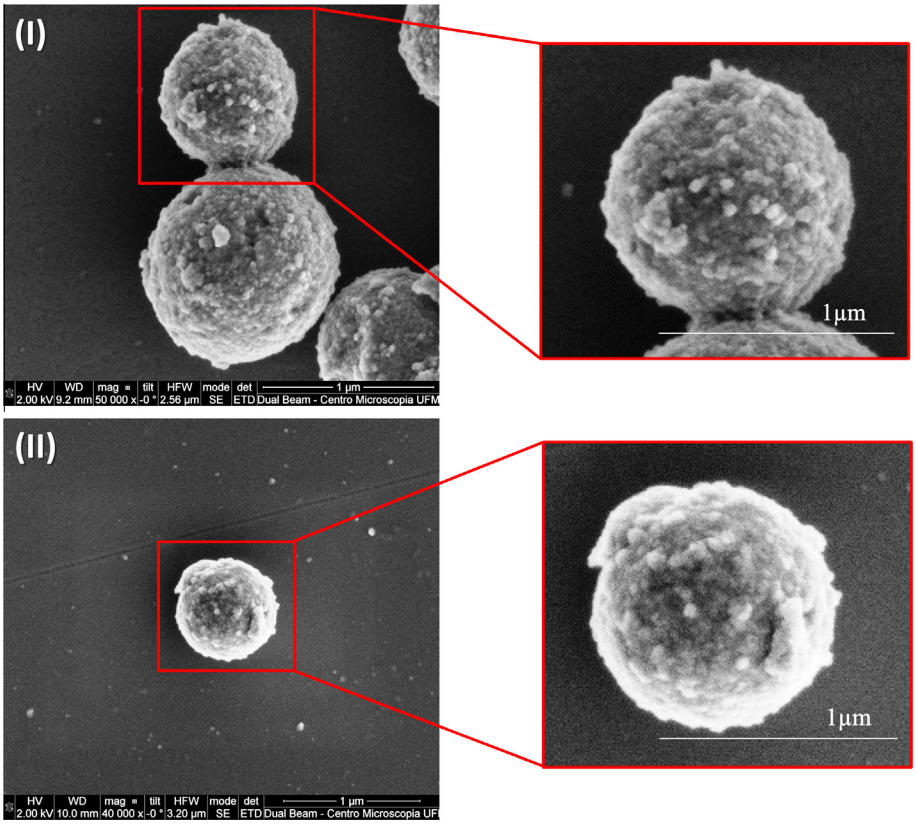

Fig. 2. SEM micrographs of titania (I) and silica–titania (II) samples in the as-prepared condition.

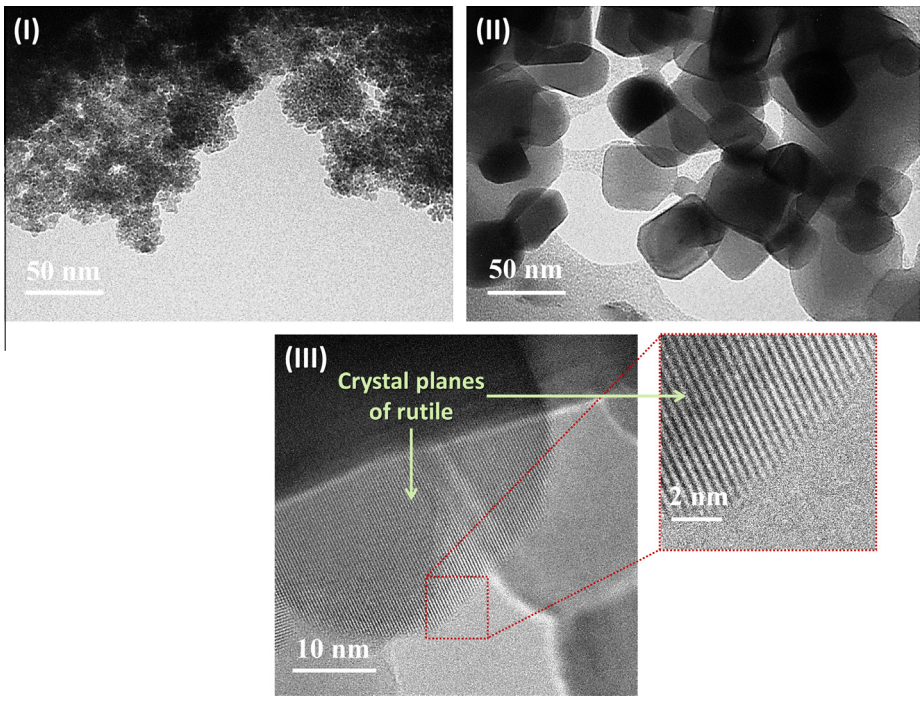

Fig. 4. TEM micrographs of TiO_2 samples. (I) TiO_2-As, (II–III) TiO_2-800.

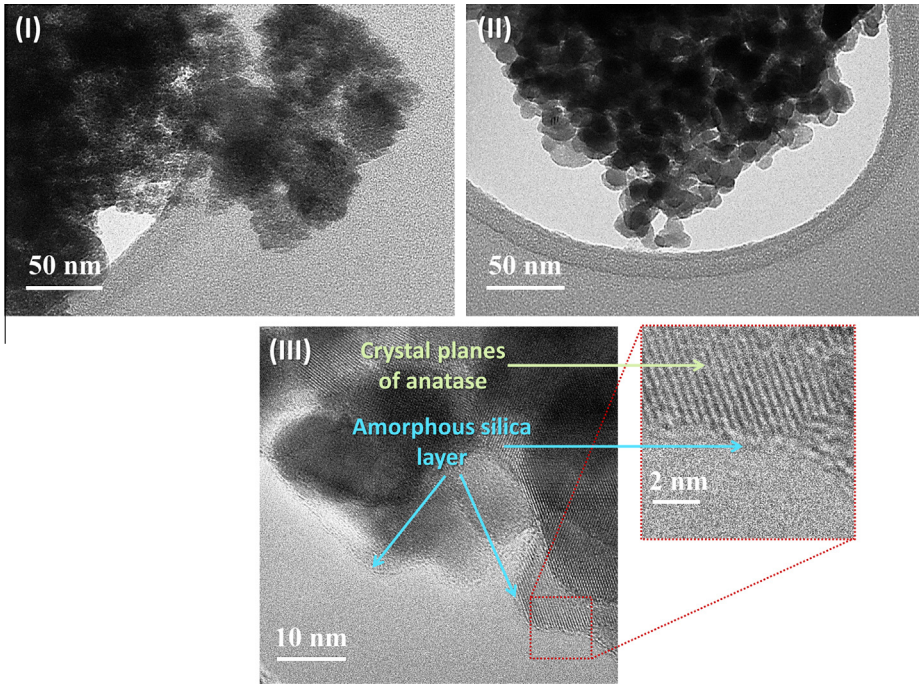

Fig. 5. TEM micrographs of TiO_2-SiO_2 samples. (I) TiO_2-SiO_2-As, (II–III) TiO_2-SiO_2-800.

noticed the existence of a homogeneous thin amorphous silica layer inferior to 1 nm enclosing the anatase particles. It is worth stressing that the TiO_2 crystallite size evaluated by the Scherrer equation is similar to that observed in the TEM examinations.

3.3. FTIR and DSC

Fig. 6 depicts FTIR spectra of pure titania and silica–titania samples. The features at about 330 cm^{-1}, 450 cm^{-1}, and 600 cm^{-1} are ascribed to Ti-O and Ti-O-Ti bonds. One notices that these bands are clearly observed in heat-treated samples. The wide band centered at about 600 cm^{-1} was slightly shifted toward higher wavenumbers upon heating pure titania at 800 °C. This behavior could be related to the conversion of anatase to rutile. Bezrodna et al. [34] reported that the shape, aggregation state and the treatment temperature of the titania particles show a significant effect on the titania spectrum. We observed that the features at 930 cm^{-1}, 1150 cm^{-1} and 1530 cm^{-1}, 1640 cm^{-1}, and 3400 cm^{-1},

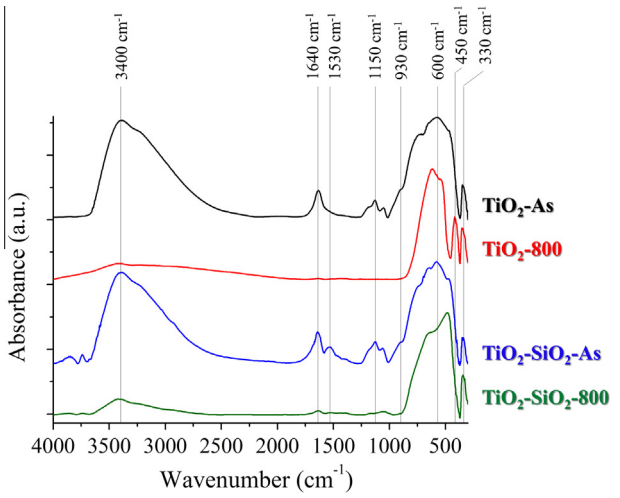

Fig. 6. FTIR spectra of TiO_2 and TiO_2-SiO_2 samples.

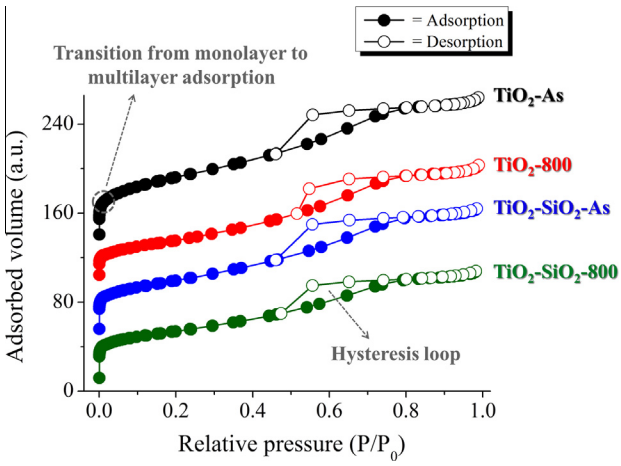

Fig. 8. N_2 sorption isotherm of TiO_2 and TiO_2-SiO_2 samples.

respectively ascribed to Ti–OH groups, organic residues, adsorbed water, and OH groups decreased significantly in intensity after the calcination step [21,35–38].

The bands at 1640 cm^{-1} and 3400 cm^{-1} showed high intensities in the spectra of the TiO_2-SiO_2 composite. This behavior could be related to the presence of Si-OH groups and chemically adsorbed water resulting from the deposition of silica on titania particles. According to Yu et al. [21], chemically adsorbed water can be observed in silica-titania samples even after their calcination at 700 °C. Features ascribed to organic residues (1150 cm^{-1} and 1530 cm^{-1}) also exhibited high intensities in the silica-titania composite. The bands ascribed to Si-O bonds are usually located at 460 cm^{-1}, 806 cm^{-1}, and 1080 cm^{-1} [39,40]. In the TiO_2-SiO_2 composite these features are superposed to those related to Ti-O bonds and organic residues. Because of this behavior it was not possible to identify the bands associated with the silica coating in the composite spectra. Only the band at 1080 cm^{-1} was observed at low intensities in the spectrum of TiO_2-SiO_2-800, which could reveal that SiO_2 is present in low proportions in the silica-titania composite.

Fig. 7 depicts the DSC profiles of TiO_2-As and TiO_2-SiO_2-As. The endothermic signal at temperatures up to 100 °C is related to the removal of physisorbed water and organic residues [41]. The exothermic peak at 250 °C may be due to the removal of TIPT residues [42]. This peak was observed in lower intensities in the composite because TIPT was widely consumed during the formation of Si-O-Ti bonds. The wide exothermic signal centered at about 400 °C observed for the TiO_2-SiO_2 composite could be associated with the removal of TEOS residues [43]. These observations are in agreement with the FTIR spectra which clearly underline the decrease of organic compounds in the pure and composite materials after the heat-treatments. Moreover, composite FTIR spectra show higher intensities of the peak assigned to organic residues as well as DSC presents an higher exothermic signal for the composite material.

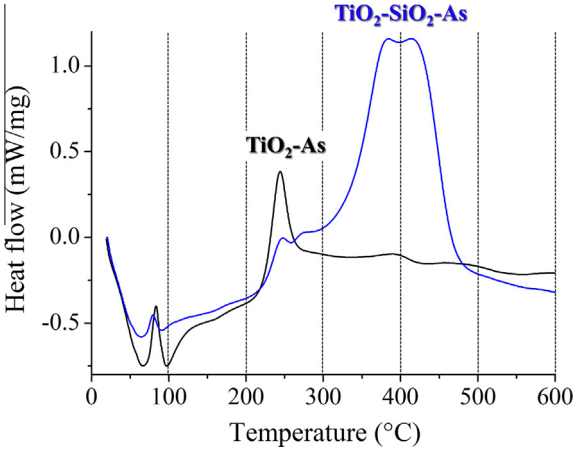

Fig. 7. DSC profiles of TiO_2 and TiO_2-SiO_2 samples in the as-prepared condition.

3.4. Nitrogen sorption tests

Figs. 8 and 9 exhibit the nitrogen sorption isotherm and pore size distribution of samples prepared in this work. Fig. 10 gives their SSA and pore volume, as-prepared titania and composite materials show high SSA about 190 and 155 m^2/g. According to IUPAC [44], the isotherms shown in Fig. 8 are associated with mesoporous materials. This type of isotherm exhibits a well-defined hysteresis loop ascribed to the capillary condensation of N_2 in mesopores. It is possible to observe the transition from monolayer to multilayer adsorption in these curves. We noticed that the hysteresis loop became narrower upon heat-treating samples at 800 °C.

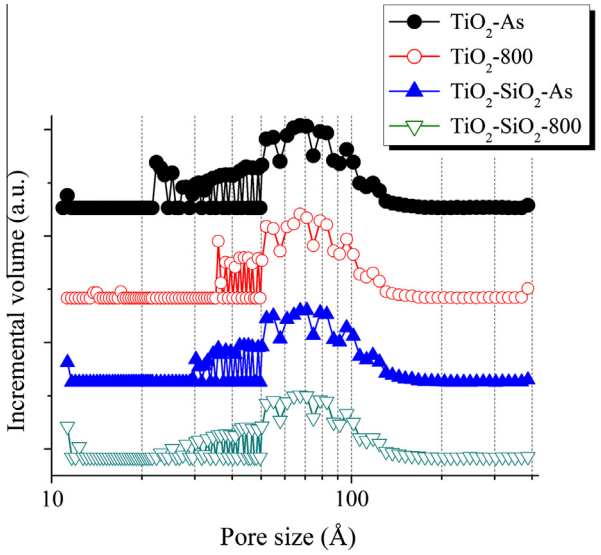

Fig. 9. Pore size distributions of TiO_2 and TiO_2-SiO_2 samples.

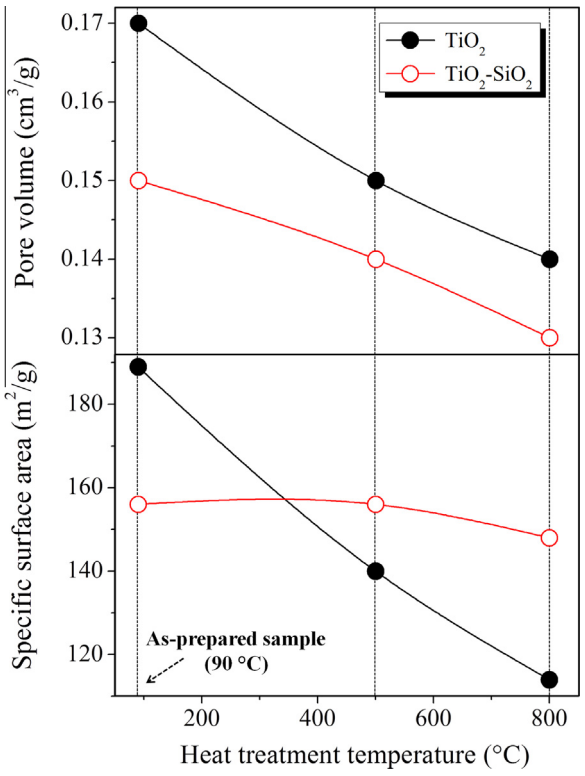

Fig. 10. SSA and pore volume of samples obtained in this work. The solid lines are used only as a guide to the eyes.

This behavior was more pronounced for pure titania indicating an higher modification of its structure along the heat treatment.

The pore size distributions depicted in Fig. 9 reveal that the samples used in this study show a small volume fraction of pores with sizes below 20 Å, which is the upper limit established by IUPAC for micropores. The calcination of samples at 800 °C shifted their pore size distributions toward larger sizes. This observation could be related to the preferential shrinkage of small pores during the heat treatment step. As a result, the closure of the small pores leads to the increase of the mean pore size. Again, this behavior was more remarkable for pure titania. From Fig. 10, we observed that the calcination step decreased both the pore volume and SSA. Pure titania showed the most significant variation in these properties. As addressed before, the deposition of a homogeneous thin SiO_2 film on TiO_2 particles inhibits their growth. This behavior contributes to the stabilization of the composite SSA at high temperatures. Moreover, the mean pore size of pure titania increased from 50 Å to 60 Å upon heat treatment. On the other hand, the mean pore size of silica–titania remained constant at 60 Å even after its calcination at either 500 °C or 800 °C. It was also observed that the silica–titania composite exhibited pore volumes lower than those shown by pure titania. This behavior could be related to the silica deposition on the titania particles. Thus, the presence of this coating could lead to a partial blockage of small pores on the titania surface.

4. Conclusions

The SiO_2-TiO_2 composite prepared in this work showed anatase as major phase. This behavior was also observed for samples in the as-prepared conditions, although the hydrothermal treatment was carried out at low temperatures (90 °C). As-prepared materials exhibited a large SSA and particle size of about 1 μm. The heat treatment of samples at 800 °C led to the removal of residual organic groups from their structures. The TiO_2 crystallite size assessed by the Scherrer equation was quite similar to that observed in TEM micrographs. We noticed that a thin and homogeneous silica layer was formed on the anatase particles. It was observed that the presence of this coating led to samples with improved thermal stability, although the studied composite presents a low SiO_2:TiO_2 molar ratio in this study. We believe that these materials show an enhanced SiO_2-TiO_2 interfacial area and a high anatase amount, which could lead to composites with interesting photoactive properties. In addition, since the SiO_2 layer seems to be very thin, the UV exposition intensity of the titania crystals would not be expected to decrease during the photocatalysis process.

Acknowledgments

The authors thank the financial support from CAPES and CNPq. We kindly acknowledge UFMG Microscopy Center and Prof. Vicente Buono for the technical support in SEM, TEM and XRD tests, respectively. The authors acknowledge the support of Dr. R. F. Martins.

References

[1] M. Wang, S. Plogmaker, R. Humphry-Baker, P. Pechy, H. Rensmo, S.M. Zakeeruddin, M. Grätzel, ChemSusChem 5 (2012) 181–187.
[2] Z. Fang, D.A. Dixon, J. Phys. Chem. A 117 (2013) 3539–3555.
[3] T.-D. Pham, B.-K. Lee, Appl. Surf. Sci. 296 (2014) 15–23.
[4] N. Lua, H.T. Yua, Yan Sud, Yan Wua, Sep. Purif. Technol. 90 (2012) 196–203.
[5] D. Ravelli, M. Fagnoni, D. Dondi, A. Albini, J. Adv. Oxid. Technol. 14 (2014) 40–46.
[6] S. Permpoon, M. Houmard, D. Riassetto, L. Rapenne, G. Berthomé, B. Baroux, J.C. Joud, M. Langlet, Thin Solid Films 516 (2008) 957–966.
[7] A. Fujishima, T.N. Rao, D.A. Tryk, J. Photochem. Photobiol., C 1 (2000) 1–21.
[8] Y.C. Lee, Y.P. Hong, H.Y. Lee, H. Kim, Y.J. Jung, K.H. Ko, H.S. Jung, K.S. Hong, J. Colloid Interface Sci. 267 (2003) 127–131.
[9] K. Guan, Surf. Coat. Technol. 191 (2005) 155–160.
[10] C. Kang, L. Jing, T. Guo, H. Cui, J. Zhou, H. Fu, J. Phys. Chem. C 113 (2009) 1006–1013.
[11] M.I. Litter, Appl. Catal. B 23 (1999) 89–114.
[12] S.C. Pillai, P. Periyat, R. George, D.E. McCormack, M.K. Seery, H. Hayden, J. Colreavy, D. Corr, J. Hinder, J. Phys. Chem. C 111 (2007) 1605–1611.
[13] J.-M. Herrmann, H. Tahiri, C. Guillard, P. Pichat, Catal. Today 54 (1999) 131–141.
[14] J. Yu, L. Zhao, B. Cheng, Mater. Chem. Phys. 96 (2006) 311–316.
[15] Z.-Y. Shen, L.-Y. Li, Y. Li, C.-C. Wang, J. Colloid Interface Sci. 354 (2011) 196–201.
[16] F.B. Li, X.Z. Li, K.H. Ng, Ind. Eng. Chem. Res. 45 (2006) 1–7.
[17] X.S. Niu, S.J. Li, H.H. Chu, J.G. Zhou, J. Rare Earth 29 (2011) 225–229.
[18] C. Zhana, F. Chena, J. Yanga, D. Daia, X. Caob, M. Zhonga, J. Hazard. Mater. 267 (2014) 88–97.
[19] A. Mahyar, M.A. Behnajady, N. Modirshahla, Indian J. Chem. A 49 (2010) 1593–1600.
[20] J.C. Yu, J. Yu, W. Ho, J. Zhao, J. Photochem. Photobiol., A 148 (2002) 331–339.
[21] J. Yu, J.C. Yu, X. Zhao, C. Zhong, J. Han, Q. Zhao, J. Mater. Sci. Lett. 20 (2001) 1745–1748.
[22] C. Huang, H. Bai, Y. Huang, S. Liu, S. Yen, Y. Tseng, Int. J. Photoenergy 1 (2012) 1.
[23] K. Guan, B. Lu, Y. Yin, Surf. Coat. Technol. 173 (2003) 219–223.
[24] S. Permpoon, G. Berthomé, B. Baroux, J.C. Joud, M. Langlet, J. Mater. Sci. 41 (2006) 7650–7662.
[25] M. Houmard, D. Riassetto, F. Roussel, A. Bourgeois, G. Berthomé, J.C. Joud, M. Langlet, Appl. Surf. Sci. 254 (2007) 1405–1414.
[26] M. Houmard, D. Riassetto, F. Roussel, A. Bourgeois, G. Berthomé, J.C. Joud, M. Langlet, Surf. Sci. 602 (2008) 3364–3374.
[27] M. Hirano, K. Ota, H. Iwata, Chem. Mater. 16 (2004) 3725–3732.
[28] A. Nilchi, S. Janitabar-Darzi, S. Rasouli-Garmarodi, Mater. Sci. App. 2 (2011) 476–480.
[29] D.S. Kim, S.-Y. Kwak, Appl. Catal. A 323 (2007) 110–118.
[30] M. Houmard, G. Berthomé, J.C. Joud, M. Langlet, Surf. Sci. 605 (2011) 456–462.
[31] H.-J. Kim, J.-D. Jeon, S.-Y. Kwak, Powder Technol. 243 (2013) 130–138.
[32] C. Xie, Z. Xu, Q. Yang, B. Xue, Y. Du, J. Zhang, Mater. Sci. Eng. B 112 (2004) 34–41.
[33] V.S. Smitha, K.A. Manjumol, K.V. Baiju, S. Ghosh, P. Perumal, K.G.K. Warrier, J. Sol–Gel. Sci. Technol. 54 (2010) 203–211.
[34] T. Bezrodna, T. Gavrilko, G. Puchkovska, V. Shimanovska, J. Baran, M. Marchewka, J. Mol. Struct. 614 (2002) 315–324.
[35] M. Burgos, M. Langlet, Thin Solid Films 349 (1999) 19–23.
[36] T. Athar, K. Han, S. Han, T. Ko, I.-M. Lee, H.-O. Yoon, Int. J. Green Nanotechnol. Mater. Sci. Eng. 1 (2009) M52–M60.

[37] D.L. Wood, E.M. Rabinovich, D.W. Johnson, J.B. MacChesney, E.M. Vogel, J. Am. Ceram. Soc. 66 (1983) 693–699.
[38] Y. Djaoued, R. Brüning, D. Bersani, P.P. Lottici, S. Badilescu, Mater. Lett. 58 (2004) 2618–2622.
[39] J. Román, S. Padilla, M. Vallet-Regí, Chem. Mater. 15 (2003) 798–806.
[40] H.Y. Jung, R.K. Gupta, E.O. Oh, Y.H. Kim, C.M. Whang, J. Non-Cryst. Solids 351 (2005) 372–379.
[41] K.N.P. Kumar, K. Keizer, A.J. Burggraaf, J. Mater. Chem. 3 (1993) 1141–1149.
[42] J.Y. Cho, W.H. Nam, Y.S. Lim, W.-S. Seo, H.-H. Park, J.Y. Lee, RSC Adv. 2 (2012) 2449–2453.
[43] A. Braem, B. Neirinck, J. Schrooten, O. Van der Biest, J. Vleugels, Mater. Sci. Eng. C 32 (2012) 2292–2298.
[44] K.S.W. Sing, D.H. Everett, R.A.W. Haul, L. Moscou, R.A. Pierotti, J. Rouquérol, T. Siemieniewska, Pure Appl. Chem. 57 (1985) 603–619.